Strojnícky časopis – *Journal of* MECHANICAL ENGINEERING,
VOL 72 (2022), NO 1, 99 – 108

# EFFECT OF LOAD ECCENTRICITY ON STRESS CONDITION OF BUTT WELDED JOINT WITH ASYMMETRICAL REINFORCEMENT

**MOLTASOV Andrii[1], TKACH Pavlo[1], USTYNENKO Oleksandr[2], PROTASOV Roman[3*]**

*[1] E.O. Paton Electric Welding Institute of the National Academy of Sciences of Ukraine, Department of Strength of Welded Structures, Kazymyra Malevycha str. 11, 03150 Kyiv, Ukraine*
*[2] National Technical University "Kharkiv Polytechnic Institute", Institute of Education and Science in Mechanical Engineering and Transport, Department of Theory and Computer-Aided Design of Mechanisms and Machines, Kyrpychova str. 2, 61002 Kharkiv, Ukraine33*
*[3*] Slovak University of Technology in Bratislava, Faculty of Mechanical Engineering, Institute of Transport Technology and Engineering Design, Nám. Slobody 17, 812 31 Bratislava, Slovakia,*
*e – mail: roman.protasov@stuba.sk*

**Abstract:** An analytical method for determination of a stress condition of butt welded thin-gauge plates with asymmetrical reinforcement is developed. The proposed method allows take into account the effect of the load application eccentricity on the tensile stress concentration factor (SCF) in the weld root zone. It is presented that the bending stresses, caused by this eccentricity, result in increasing the total stresses up to 75%. The results of analytical SCF calculations are in good agreement with the results obtained using the finite element method.

**KEYWORDS:** butt welded joint, asymmetrical reinforcement, stress condition, stress concentration, root reinforcement, load eccentricity, nonplanar section hypothesis.

## 1 Introduction

Welding is applicable for manufacturing and repair of different constructions. It allows join rigidly the elements made of steel [1] aluminium [2] plastic [3] and other materials. TIG and MIG welding processes, due to their advantages, are widely used for joining the metal elements in many industries. At the same time, they provide geometrical shape change which causes increasing of the stresses in the transition zone from the weld to the base metal. This phenomenon known as stress concentration is one of the main factors which determine the fatigue life of welded joints [4]. It is well known that stress concentration should be taken into account not only under vibration, but also under static loading, when brittle fracture is possible. The tests of high-strength D16T1 Al-alloy (similar to EN AW-2024 alloy) and 1460T1 alloy of Al-Cu-Li system butt welded joints under the uniaxial static tension show that failure occurs in the zone of fusion of the weld metal with the base metal, where the maximum level of stress concentration takes place [5]. These results can be explained by the brittleness of the joint zone due to structural transformation in the heat-hardened aluminium alloys under the influence of the thermal cycle of fusion welding [6].

The problem of assessment of the carbon steels and aluminium alloys welded joints durability taking into account all design and technological features can be partially solved using File Allocation Table (FAT) catalogues. They include series of fatigue curves obtained as a result of endurance testing of real welded elements and expressed in terms of stress ranges, regardless of the load application cycle asymmetry factor. However, calculations by nominal stresses for welded structures in some cases leads to ~~the~~ premature appearance of the

DOI: 10.2478/scjme-2022-0010, Print ISSN 0039-2472, On-line ISSN 2450-5471

fatigue cracks. That is why they require additional corrections which allow take into account the stress concentration in local zones [7].

Modern approaches to the assessment of welded structures fatigue life characteristics involve the calculation of nominal stresses near welds using the finite element method (FEM) with subsequent multiplication by the SCF calculated by the corresponding formulas [8].

The literature review [9] shows that the currently available formulas for determining the SCF of butt welded joints are intended for welds with one-side or symmetrical double-side reinforcement, while the butt welded joints with asymmetrical double-side reinforcement are ignored. In addition, the range of applicability of the available formulas precludes their use for determining the SCF for welded thin-gauge plates. Therefore, the development of analytical methods for the stress condition assessment of the butt welded thin-gauge plates with different size of the face and root reinforcements is justified in [9] as a topical subject for further research.

The work [10] is concentrated on solution of this problem. According to the results of [10] it was found that due to the reinforcement cross section increases on the face side, the stresses in the root part of the butt welded joint with asymmetrical reinforcement decrease. However, the proposed in [10] method does not take into account the bending stresses caused by the eccentricity of the tensile load application. These stresses cause changes in stress condition of the joint as follows: the face side total stress decreases and root side total stress increases [11]. This is confirmed by the tests of samples of 1460 Al-alloy butt joints, welded by TIG welding. The failure of samples under the uniaxial static tension according to [12] occurred in the transition zone from the weld root reinforcement to the base metal. Therefore, development of an integrated approach to assessment of the influence of face-side reinforcement geometry on the root side stress condition is relevant.

## 2 Hypothesis description

Draw a nonplanar section *ABC* through point *A* (Fig. 1) according to the rules [13].

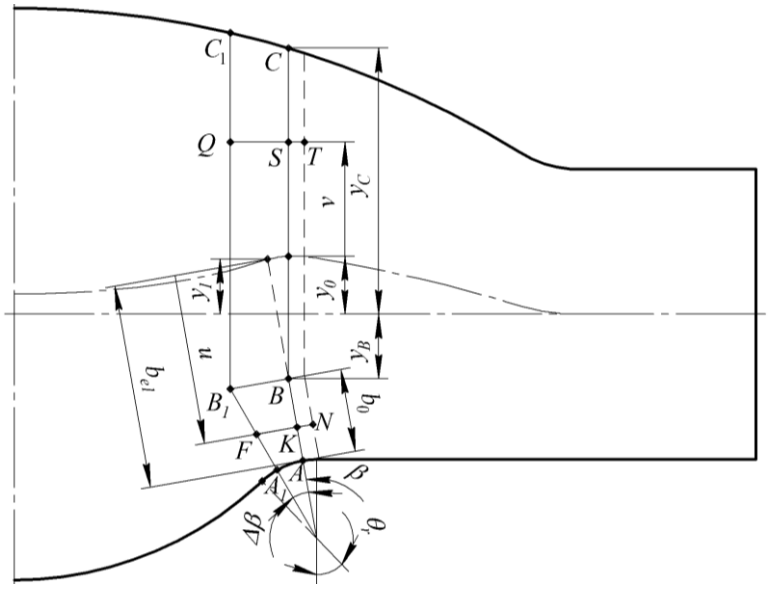



Fig. 1 Configuration of nonplanar sections in the root-side transition zone

The part of section *AB* is perpendicular to the contour, and its length is equal to depth $b_0$ of the stress concentration action, while section *BC* is perpendicular to the line of the load action. Following the same rule, draw a nonplanar section $A_1B_1C_1$ through the point $A_1$ in a way that the continuations of the segments *AB* and $A_1B_1$ form an infinitely small angle $\Delta\beta$ (Fig. 1).

When using the idealized model which is shown in Fig. 2 for defining the reinforcement geometry by the arcs of contiguous circles, depth $b_0$ can be determined according to the results of [10]

$$b_0 = 4r_r h_r \sqrt{\frac{2}{g_r^2+4h_r^2}},$$

where $r_r$ is the radius of transition from the weld root reinforcement to the base metal; $g_r$ and $h_r$ are the width and height of the root reinforcement, respectively.

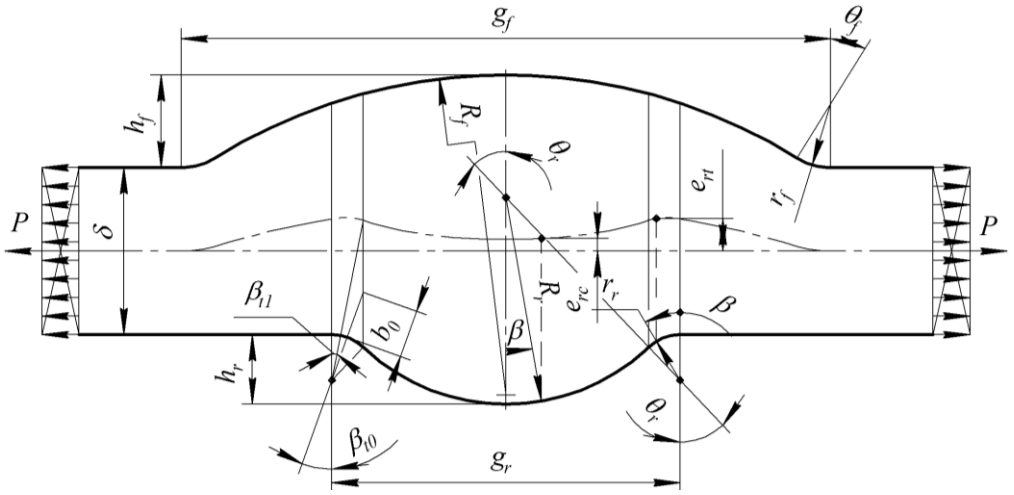



Fig. 2 Geometric parameters of the idealized model of the asymmetrical butt welded joint

## 3 Tension

According the results obtained in [10], due to displacement of the section *ABC* to the position indicated in Fig. 1 by the dotted line, normal tensile stresses arise in the *KF* and *QS* fibers. They can be obtained as:

$$\sigma_u^T = \frac{KN \cdot E}{(r_r+b_{e1}-u)\cdot \Delta\beta},\ \sigma_v^T = \frac{KN \cdot E}{(r_r+b_0)\cdot \Delta\beta},\ \text{where } b_{e1} = \frac{\delta+2y_1+2r_r\cdot(1-\cos\beta)}{2\cos\beta}. \quad (1)$$

It should be mentioned that geometric characteristics $b_{e1}$ from Eq. (1) and $b_1$ from [10] are different. Geometric characteristic $b_{e1}$ contains parameter $y_1$, which takes into account the distance between the load application axis and the section center of inertia (Fig. 1).

If the continuation of segment *AB* intersects the centers-of-inertia line in the concave part of the root reinforcement, this is equally matched to the condition:

$$\beta \le \beta_{t1} = arctan \frac{2r_r \cdot sin\theta_r}{\delta+h_f-R_f+r_r(1+cos\theta_r)+\sqrt{R_f^2-\left(r_r\cdot sin\theta_r-\frac{g_r}{2}\right)^2}}, \quad (2)$$

where δ is the thickness of the base metal; $h_f$ is the height of the face reinforcement; $R_f$ is the radius of its convex part and $\theta_r$ is the flank angle on the root side of the weld (Fig. 2).

In this case, parameter $y_1$ can be calculated by the formula:

$$y_1 = \frac{1}{2}\left(\sqrt{\frac{C_{t3}^2}{4}-C_{t2}+\Psi_t}-\frac{C_{t3}}{2}+\sqrt{\left(\frac{C_{t3}}{2}-\sqrt{\frac{C_{t3}^2}{4}-C_{t2}+\Psi_t}\right)^2+4\sqrt{\frac{\Psi_t^2}{4}-C_{t0}}-2\Psi_t}\right)$$

where $C_{t3} = \frac{2(2r_r+\delta-H_t)\cdot tan^2\beta-g_r\cdot tan\beta-4H_t}{2(1+tan^2\beta)}$; $H_t = h_f - R_f - r_r$; $K_t = R_f^2 - r_r^2 - \frac{g_r^2}{4}$;

$$C_{t2} = \frac{\left(4\left[(H_t-2r_r-\delta)^2-2H_t\cdot(2r_r+\delta)\right]+g_r^2\right)tan^2\,\beta+8g_r\left(H_t-r_r-\frac{\delta}{2}\right)tan\,\beta-8\left(2r_r^2+K_t-3H_t^2\right)}{16(1+tan^2\,\beta)};$$

$$C_{t0} = \frac{\left(4H_t^2+g_r^2\right)\cdot\left(r_r+\frac{\delta}{2}\right)^2\cdot tan^2\,\beta+2g_r\cdot\left(K_t-H_t^2\right)\cdot\left(r_r+\frac{\delta}{2}\right)\cdot tan\,\beta-2\left(2r_r^2+K_t\right)\cdot H_t^2+K_t^2+H_t^4}{16(1+tan^2\,\beta)};$$

$$\Psi_t = \frac{C_{t2}}{3}+\sqrt[3]{-\frac{C_{tq}}{2}+\sqrt{\frac{C_{tq}^2}{4}+\frac{C_{tp}^3}{27}}}+\sqrt[3]{-\frac{C_{tq}}{2}-\sqrt{\frac{C_{tq}^2}{4}+\frac{C_{tp}^3}{27}}}; \quad (3)$$

$$C_{tp} = -\frac{C_{t2}^2}{3}+C_{t1}\cdot C_{t3}-4C_{t0};\; C_{tq} = -\frac{2C_{t2}^3}{27}+\frac{1}{3}C_{t1}\cdot C_{t2}\cdot C_{t3}+\frac{8C_{t0}}{3}\cdot C_{t2}-C_{t0}\cdot C_{t3}^2-C_{t1}^2;$$

$$C_{t1} = \frac{\left(4H_t^2-8H_t\cdot\left(r_r+\frac{\delta}{2}\right)+g_r^2\right)\cdot\left(r_r+\frac{\delta}{2}\right)\cdot tan^2\,\beta+g_r\cdot\left(4H_t\cdot\left(r_r+\frac{\delta}{2}\right)-H_t^2+K_t\right)\cdot tan\,\beta+4H_t\cdot\left(2r_r^2+K_t-H_t^2\right)}{8(1+tan^2\,\beta)}.$$

If condition of Eq. (2) is not fulfilled (the continuation of segment *AB* crosses the centers-of-inertia line on the convex part of the root reinforcement), then:

$$y_1 = \frac{1}{2}\left(\sqrt{\frac{C_{c3}^2}{4}-C_{c2}+\Psi_c}-\frac{C_{c3}}{2}-\sqrt{\left(\frac{C_{c3}}{2}-\sqrt{\frac{C_{c3}^2}{4}-C_{c2}+\Psi_c}\right)^2+4\sqrt{\frac{\Psi_c^2}{4}-C_{c0}}-2\Psi_c}\right).$$

Parameter $\Psi_c$ is defined similarly to $\Psi_t$ with appropriate replacement of $C_{tq}$, $C_{tp}$, $C_{t0}$, …, $C_{t3}$ by $C_{cq}$, $C_{cp}$, $C_{c0}$, …, $C_{c3}$ in Eq. (3):

$$C_{cp} = -\frac{C_{c2}^2}{3}+C_{c1}\cdot C_{c3}-4C_{c0};\; C_{cq} = -\frac{2C_{c2}^3}{27}+\frac{1}{3}C_{c1}\cdot C_{c2}\cdot C_{c3}+\frac{8C_{c0}}{3}\cdot C_{c2}-C_{c0}\cdot C_{c3}^2-C_{c1}^2;$$

$$C_{c0} = \frac{4H_c^2\cdot\left(r_r+\frac{\delta}{2}\right)^2\cdot tan^2\,\beta-4g_r\cdot H_c^2\cdot\left(r_r+\frac{\delta}{2}\right)\cdot tan\,\beta+\left(2K_c+H_c^2-4R_f^2+g_r^2\right)\cdot H_c^2+K_c^2}{16(1+tan^2\,\beta)};$$

$$C_{c1} = \frac{H_c\cdot\left[2\left(r_r+\frac{\delta}{2}\right)\cdot(H_c+2r_r+\delta)\cdot tan^2\,\beta-g_r\cdot(H_c+4r_r+2\delta)\cdot tan\,\beta+\left(2K_c+2H_c^2-4R_f^2+g_r^2\right)\right]}{4(1+tan^2\,\beta)};$$

$$C_{c2} = \frac{\left[(H_c+2r_r+\delta)^2+2H_c\cdot(2r_r+\delta)\right]\cdot tan^2\,\beta-4g_r\cdot\left(H_c+r_r+\frac{\delta}{2}\right)\cdot tan\,\beta+2K_c+6H_c^2-4R_f^2+g_r^2}{4(1+tan^2\,\beta)};$$

$$C_{c3} = \frac{(2r_r+\delta+H_c)\cdot tan^2\,\beta-g_r\cdot tan\,\beta+2H_c}{1+tan^2\,\beta};\; H_c = R_f-h_f-R_r+h_r;\; K_c = R_f^2-R_r^2,$$

where $R_r$ is the radius of the face reinforcement convex part.

The equilibrium condition for the joint of unit thickness has the form

$$P = \int_{b_{e1}-b_0}^{b_{e1}}\sigma_u^T du\cdot cos\,\beta+\int_{-y_B-y_0}^{y_C-y_0}\sigma_v^T dv, \quad (4)$$

where $y_B$ and $y_C$ can be defined as:

$$y_B = \frac{\delta}{2}+r_r(1-cos\,\beta)-b_0\,cos\,\beta;\; y_C = \frac{\delta}{2}+h_f-R_f+\sqrt{R_f^2-\left[(r_r+b_0)\,sin\,\beta-\frac{g_r}{2}\right]^2}. \quad (5)$$

Parameter $y_0$ in Eq. (4) also takes into account the distance between the load application axis and the section center of inertia.

Segment *BC* can intersect the centers-of-inertia line in the concave part of the root reinforcement. This is equally matched to the condition:

$$\beta \le \beta_{t0} = arcsin\frac{r_r \cdot sin\theta_r}{r_r + b_0}. \quad (6)$$

In this case parameter $y_0$ can be calculated by the formula:

$$y_0 = \frac{h_f - R_f - r_r + \sqrt{R_f^2 - \left[(r_r + b_0)\sin\beta - \frac{g_r}{2}\right]^2} + \sqrt{r_r^2 - (r_r + b_0)^2 \sin^2\beta}}{2}.$$

If condition (6) is not fulfilled and segment *BC* intersects the centers-of-inertia line in the convex part of the root reinforcement, then:

$$y_0 = \frac{h_f - R_f - h_r + R_r + \sqrt{R_f^2 - \left[(r_r + b_0)\sin\beta - \frac{g_r}{2}\right]^2} - \sqrt{R_r^2 - \left[(r_r + b_0)\sin\beta - \frac{g_r}{2}\right]^2}}{2}.$$

Substituting expressions for stresses (1) into equilibrium condition (4), after integration we obtain

$$\frac{P}{T_0} = \frac{KN \cdot E}{\Delta\beta}, \quad (7)$$

where $T_0 = \cos\beta \cdot ln\frac{r_r + b_0}{r_r} + \frac{y_C + y_B}{r_r + b_0}$ is the geometric characteristic of a nonplanar section under tensile loading which varies from section to section.

Substituting identity (7) into formulas (1), functional connection between the tensile force *P* and the stresses in sections *AB* and *BC* is as follows:

$$\sigma_u^T = \frac{P}{(r_r + b_{e1} - u)\cdot T_0},\ \sigma_v^T = \frac{P}{(r_r + b_0)\cdot T_0}. \quad (8)$$

From the analysis of second Eq. (8) it follows that in section *BC* the through-the-thickness stress is constant, and it changes only from section to section. Therefore, the stresses on the contour of the face reinforcement (point *C*) under tensile loading are determined by the formula $\sigma_f^T = \sigma_v^T$.

At the same time, according to first Eq. (8), the stress in section *AB* changes according to hyperbolic law and reaches its maximum at point *A*, i.e. on the surface of the transition zone from the weld root to the base metal at $u = b_{e1}$. The stresses on the root side of the joint under tensile loading can be determined by the following formula:

$$\sigma_r^T = \frac{P}{r_r \cdot T_0}. \quad (9)$$

The obtained formulas are valid for the case of fulfilling the condition $b_0 \le b_{e1}$. If $b_0 > b_{e1}$, then in second Eq. (1), Eqs. (4) and (5) one should take $b_0 = b_{e1}$ and $y_0 = y_1$. In this case the lower limits of both integrals (4) vanish and the geometric characteristic of nonplanar sections under tensile loading is determined as follows: $T_1 = \cos\beta \cdot ln\frac{r_r + b_{e1}}{r_r} + \frac{y_C - y_1}{r_r + b_{e1}}$. The stresses on the front and root surfaces of the joint are as follows:

$$\sigma_f^T = \frac{P}{(r_r + b_{e1})\cdot T_1},\ \sigma_r^T = \frac{P}{r_r \cdot T_1}. \quad (10)$$

## 4 Bending

As mentioned before, bending stresses appear in addition to the axial tension stresses due to the action of the bending moment of the force *P* in the butt weld reinforcement. This moment is caused by the eccentricity $e_{rt}$ (Fig. 2) of the tensile load application on the concave part of the root reinforcement. Thus, the bending moment can be defined as $M = P \cdot e_{rt}$. According to the accepted geometric model (Fig. 2), the eccentricity is as follows:

$$e_{rt} = \frac{1}{2}\left[h_f - R_f + \sqrt{R_f^2 - \left(r_r \sin\beta - \frac{g_r}{2}\right)^2} - r_r(1 - \cos\beta)\right].$$

Assume that section $A_1B_1C_1$ under the bending loading remains stationary, while section *ABC* rotates by a small angle $\Delta\gamma$ and occupy a new position which is indicated in Fig. 3 by the dotted line. In this case, fiber *KF* , which locates at the distance $u$ from the section center of inertia, will be elongated by the length of segment $KN = [(y_B + y_0)/\cos\beta + u - b_{e1} + b_0]\tan\Delta\gamma$ (Fig. 1 and Fig. 3).

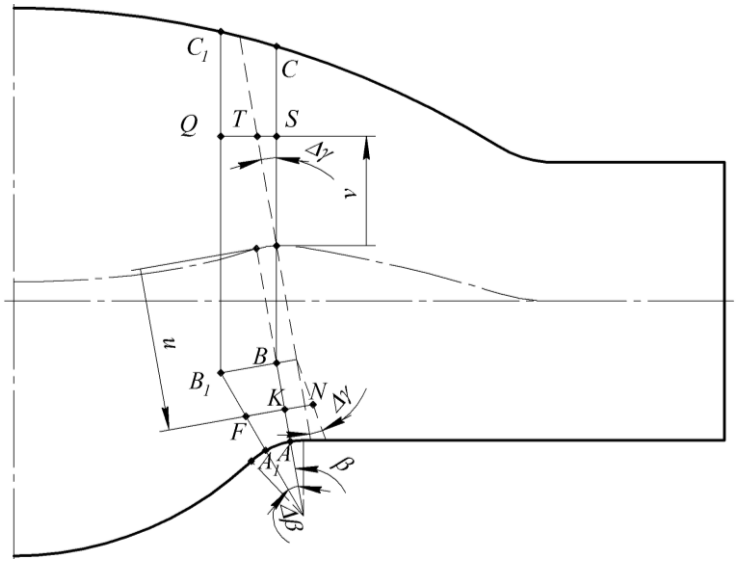



Fig. 3. Rotation of nonplanar section ABC of a butt weld at bending

As a result, the normal tensile stress will appear in it. At the same time, fiber *QS* which locates at a distance $v$ from the section center of inertia, will be shortened by the length of segment *ST* , and the normal compressive stress will appear in it. The stresses in fibers *KF* and *QS* are as follows:

$$\sigma_u^B = \frac{\left(\frac{y_B+y_0}{\cos\beta}+u-b_{e1}+b_0\right)\cdot\Delta\gamma\cdot E}{(r_r+b_{e1}-u)\cdot\Delta\beta}, \sigma_v^B = \frac{v\cdot\Delta\gamma\cdot E}{(r_r+b_0)\cdot\Delta\beta\cdot\cos\beta}. \quad (11)$$

The equilibrium condition for the joint of unit thickness under bending loading has the following form:

$$M = \int_{b_{e1}-b_0}^{b_{e1}} \sigma_u^B \cdot \left(\frac{y_B+y_0}{\cos\beta} + u - b_{e1} + b_0\right) du + \int_{-y_B-y_0}^{y_C-y_0} \sigma_v^B \cdot v dv. \quad (12)$$

Substitute Eqs. (11) into equilibrium condition (12) and after integration we obtain:

$$\frac{M}{B_0} = \frac{\Delta\gamma\cdot E}{\Delta\beta}, \quad (13)$$

where $B_0$ is the geometric characteristic of a nonplanar section under bending loading which varies from section to section

$$B_0 = \frac{(y_B+y_0-(b_{e1}-b_0)\cos\beta)^2}{\cos^2\beta}\cdot ln\frac{r_r+b_0}{r_r} + (r_r+b_{e1})^2\, ln\frac{r_r+b_0}{r_r} - b_0(r_r+2b_{e1}) + \frac{b_0^2}{2} +$$
$$+\frac{2(y_B+y_0-(b_{e1}-b_0)\cos\beta)}{\cos\beta}\left[(r_r+b_{e1})\, ln\frac{r_r+b_0}{r_r} - b_0\right] + \frac{(y_C-y_0)^3+(y_B+y_0)^3}{3(r_r+b_0)\cos\beta}.$$

Substitute identity (13) into Eq. (11) and establish the functional connection between the bending moment *M* and the stresses in sections *AB* and *BC*, respectively:

$$\sigma_u^B = \frac{M\cdot\left(\frac{y_B+y_0}{\cos\beta}+u-b_{e1}+b_0\right)}{(r_r+b_{e1}-u)\cdot B_0},\ \sigma_v^B = \frac{M\cdot v}{(r_r+b_0)\cdot B_0\cdot\cos\beta} \quad (14)$$

Obtain from Eq. (14) at $u = b_{e1}$ and $v = y_C - y_0$ the bending stresses which act in the transition zone from the weld root to the base metal (point *A*) and on the face reinforcement (point *C*) as follows:

$$\sigma_r^B = \frac{M\cdot(y_B+y_0+b_0\cdot\cos\beta)}{r_r\cdot B_0\cdot\cos\beta},\ \sigma_f^B = \frac{M\cdot(y_C-y_0)}{(r_r+b_0)\cdot B_0\cdot\cos\beta}. \quad (15)$$

These formulas are valid for the case of fulfilling the condition $b_0 \le b_{e1}$. If $b_0 > b_{e1}$, then in second Eq. (11) and condition (12) one should take $b_0 = b_{e1}$ and $y_0 = y_1$.Thus, the stresses at points *A* and *C* will be determined as:

$$\sigma_r^B = \frac{M\cdot b_{e1}}{r_r\cdot B_1},\ \sigma_f^B = \frac{M\cdot(y_C-y_1)}{(r_r+b_{e1})\cdot B_1\cdot\cos\beta}. \quad (16)$$

where $B_1$ is the geometric characteristic of a nonplanar section under bending loading which varies from section to section. In the case of fulfilling the condition $b_0 \ge b_{e1}$ it is as follows:

$$B_1 = (r_r + b_{e1})^2\, ln\frac{r_r+b_{e1}}{r_r} - b_{e1}(r_r + 2b_{e1}) + \frac{b_{e1}^2}{2} + \frac{(y_C-y_1)^3}{3(r_r+b_{e1})\cos\beta}.$$

In the case of fulfilling the condition $b_0 \le b_{e1}$, the total stresses $\sigma_r^\Sigma$ which act in the transition zone from the weld root to the base metal under the tensile and bending loadings can be calculated as the sum of the stresses obtained by Eq. (9) and first Eq. (15). On the contour of the face reinforcement the total stresses $\sigma_f^\Sigma$ under the tensile and bending loadings can be calculated as the difference between the stresses obtained by second Eq. (8) and second Eq. (15). They are as follows:

$$\sigma_r^\Sigma = \frac{P}{r_r}\left(\frac{1}{T_0} + \frac{e_{rt}\cdot(y_B+y_0+b_0\cdot\cos\beta)}{B_0\cdot\cos\beta}\right),\ \sigma_f^\Sigma = \frac{P}{(r_r+b_0)}\left(\frac{1}{T_0} - \frac{e_{rt}\cdot(y_C-y_0)}{B_0\cdot\cos\beta}\right). \quad (17)$$

In the case of fulfilling the condition $b_0 \ge b_{e1}$, total stresses $\sigma_r^\Sigma$ can be calculated as the sum of the stresses obtained by second Eq. (10) and first Eq. (16); total stresses $\sigma_f^\Sigma$ can be calculated as the difference between the stresses obtained by first Eq. (10) and second Eq. (16):

$$\sigma_r^\Sigma = \frac{P}{r_r}\left(\frac{1}{T_1} + \frac{e_{rt}\cdot b_{e1}}{B_1}\right),\ \sigma_f^\Sigma = \frac{P}{(r_r+b_{e1})}\left(\frac{1}{T_1} - \frac{e_{rt}\cdot(y_C-y_1)}{B_1\cdot\cos\beta}\right). \quad (18)$$

## 5 Calculation example and results analysis

Consider the AMg6M aluminium alloy TIG-welded butt joints which was welded using 1.6 mm welding wire SvAMg6. The thickness of welded plates is 1.8 mm and joint geometrical shape is presented in work [14]. The geometric parameters of the weld according to the idealised model are listed below.

| Side | Heigth *h*, mm | Width *g*, mm | Angle $\theta$, º | Radius *r*, mm | Radius *R*, mm | Depth $b_0$, mm |
|---|---|---|---|---|---|---|
| Face (f) | 1.000 | 7.000 | 31.890 | 0.690 | 5.935 | 0.536 |
| Root (r) | 0.750 | 3.750 | 43.602 | 0.490 | 2.229 | 0.515 |

The values of the flank angles $\theta$ are calculated according to the formulas of [15]. The radii *r* of transition from the weld to the base metal are calculated according to the formulas of [16], and the radii *R* of the convex parts of the reinforcement are calculated according to the formulas of [10].

Build the stress diagrams on the joint front and root sides (Fig. 4). Solid lines in Fig. 4 indicate the total stresses calculated taking into account the eccentricity of the load

application. Dashed lines indicate the total stresses calculated without taking into account the eccentricity of the load application.

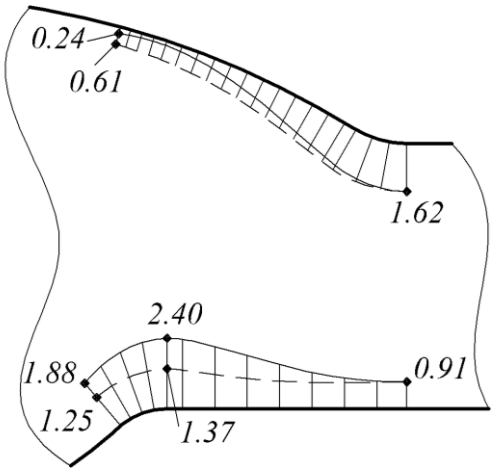



Fig. 4. Stress diagrams on the front and root sides of the AMg6M alloy welded joint

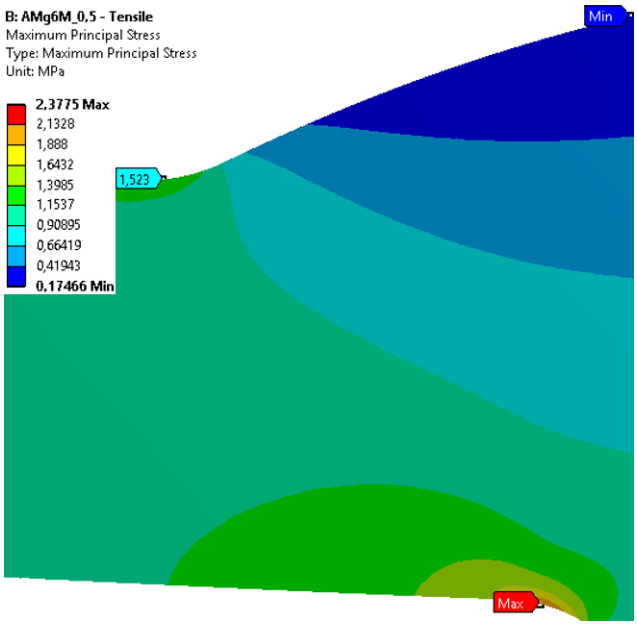



Fig. 5. The results of stress fields numerical simulation in AMg6M alloy butt welded joint

At the foot of the weld transition zone from the root reinforcement to the base metal the condition $b_0 \leq \delta/2$ is fulfilled at $\beta = 0$. In addition, since the condition $b_0 \leq b_{e1}$ is fulfilled at $0 \leq \beta \leq \theta_r$, the diagrams are built according to Eq. (17). The stress diagrams in sections corresponding to the transition zone from the weld face reinforcement to the base metal are built according to the formulas of [17]. Analysis of the diagrams presented in Fig. 4 shows that the eccentricity of the load application leads to the stresses increasing by 75% at the foot of the weld transition zone from the root to the base metal. As a result, the maximum stress value in the root side is higher than that in the face side. Note that if to disregard the eccentricity of the load application, the maximum stress value in the face side is higher.

To verify the results obtained by the developed method, computer simulation of stress fields in the test sample was carried out using the finite element method (FEM). The used mesh was refined until the difference between the stress values in the final and previous model was obtained, not exceeding 5%. In this case, according to [18], the influence of its dimensions on the values of local maximum stresses is excluded. As a result, the final model included 172035 elements with 688802 nodes. At the same time, the element size in the transition zones from the weld to the base metal was less than 0.1 of the transition radius.

The deviations of the maximum stress values obtained by the analytical and numerical calculations is less than 1% on the root side, and it is about 6% on the face side. The stresses distribution along the joint contour is the same. The maximum stress according to the analytical calculation (Fig. 4) acts at the foot of the transition zone from the weld root to the base metal at $\beta = 0$. This is also confirmed by the results of the computer simulation of stress fields which is shown in Fig. 5, this is why it makes sense to determine the SCF at this point.

For the case of fulfilling the condition $b_0 \leq b_{e1}$, the SCF is defined as the ratio of the stress determined by first Eq. (17) at $\beta = 0$ to the nominal stress $\sigma_{nom} = P/\delta$ which acts at a

sufficient distance from the weld. Considering that for the section $\beta = 0$ we have $y_1 = y_0$ and $b_{e1} = \delta/2 + y_0$ , we obtain:

$$\alpha_\sigma^r = \frac{\delta}{r_r}\left(\frac{1}{ln\frac{r_r+b_0}{r_r}+\frac{m-b_0}{r_r+b_0}} + \frac{m\cdot(m-\delta)}{4\left[\left(r_r+\frac{m}{2}\right)^2 ln\frac{r_r+b_0}{r_r}-b_0\cdot(r_r+m)+\frac{b_0^2}{2}+\frac{m^3+(m-2b_0)^3}{24(r_r+b_0)}\right]}\right), \quad (19)$$

where $m = \delta + h_f - R_f + \sqrt{R_f^2 - g_r^2/4}$. If the condition $b_0 \geq b_{e1}$ is fulfilled the SCF is defined as the ratio of the stress determined by first Eq. (18) at $\beta = 0$ to the nominal stress:

$$\alpha_\sigma^r = \frac{\delta}{r_r}\left(\frac{1}{ln\frac{2r_r+m}{2r_r}+\frac{m}{2r_r+m}} + \frac{m\cdot(m-\delta)}{4\left[\left(r_r+\frac{m}{2}\right)^2 ln\frac{2r_r+m}{2r_r}-\frac{m}{2}\cdot(r_r+m)+\frac{m^2}{8}+\frac{m^3}{12(2r_r+m)}\right]}\right). \quad (20)$$

Thus, Eqs. (19) and (20) establish the functional connection between the SCF value on the root side and the geometric dimensions of reinforcements both on the front and root sides of the butt welded joint with asymmetrical reinforcement.

## CONCLUSION

The functional connection between the SCF value at the transition zone from the weld root to the base metal and the geometric parameters of the reinforcements on either side of the butt welded joint is obtained. The analytical method for the stress condition assessment under tensile loading in the stress concentration zones of the butt welded joint with asymmetrical reinforcement is developed and verified. The following conclusions can be drawn:

1. Obtained formulas take into account the increasing of the cross section due to the reinforcement on the face side and the eccentricity of the tensile load application. This is why developed method allows ~~to~~ obtain more accurate stresses value due to the influence of the load application eccentricity on the stress distribution in the transition zone from the weld root to the base metal.

2. The results of calculations by the method show that the bending stresses caused by eccentricity of the tensile load application lead to increasing by 75% of the total stress in the root part of butt welded thin-gauge plates with asymmetrical reinforcement. The obtained results agree well with the results of stress numerical analysis. The maximum stress values obtained using the FEM differ from those calculated in the following way: on the root side by 1% and on the face side by 6%.

## REFERENCES


[1] Moi Subhas, Ch., Ramesh, R., Kumar, P. P., Asish, B. “Analysis of Impact Behaviour of TIG Weldment by Using Hybrid RSM and CSO”, Strojnícky časopis – Journal of Mechanical Engineering 69 (4), pp. 105 – 114, **2019**. DOI: 10.2478/scjme-2019-0046

[2] Srinivasa Rao, M., Tangudu S. S., Perumalla, S., Uppda, B. R., Yandra, Ch., Kambhampati, K. “Effect of TIG and FSW Welding Processes on Mechanical Properties of Al-4.2Mg-0.6Mn-0.4Sc-0.1Zr Alloy”, Strojnícky časopis – Journal of Mechanical Engineering 71 (2), pp. 299 – 304, **2021**. DOI: 10.2478/scjme-2021-0036

[3] Kovalchuk, M., Iurzhenko, M., Demchenko, V., Senchenkov, I. “The Investigation of the Welding Process of Different-Type Polyethylenes”, In: Pogrebnjak, A., Novosad, V. (eds) Advances in Thin Films, Nanostructured Materials, and Coatings. Lecture Notes in Mechanical Engineering. Springer, Singapore, **2019**. DOI: 10.1007/978-981-13-6133-3_23

[4] Skriko, T., Ahola, A. & Björk, T. “Overview on the digitized production of welded steel structures”, Welding in the World, **2022**. DOI: 10.1007/s40194-021-01224-x

[5] Klochkov, I., Poklaytsky, A., Motrunich, S. “Fatigue behavior of high strength Al-Cu-Mg and Al-Cu-Li alloys joints obtained by fusion and solid state welding technologies”, Journal of Theoretical and Applied Mechanics 49(2), pp. 179 – 189, **2019**. DOI: 10.7546/JTAM.49.19.02.07

[6] Poklyatsky, A. G., Knysh, V. V., Klochkov, I. N., Motrunich, S. I. “Features and advantages of the process of friction stir welding of butt joints of sheet aluminum-lithium alloys”, The Paton Welding Journal 5 – 6, pp. 86 – 90, **2016**. DOI: 10.15407/as2016.06.15

[7] Hobbacher, A. F. “Recommendations for fatigue design of welded joints and components”, IIW Collection, 2nd Edition, series Editor Cècile Mayer, Springer International Publishing, Villepinte, France, **2016**. DOI: 10.1007/978-3-319-23757-2

[8] Goyal, R., El-Zein, M., Glinka, G. “A robust stress analysis method for fatigue life prediction of welded structures”, Welding in the World 60(2), pp. 299 – 314, **2016**. DOI: 10.1007/s40194-016-0295-y

[9] Tkach, P. N., Moltasov, A. W. “Development of Methods for the Assessment of Stresses in Welded Structure Elements: Part 2. The Latest Methods”, Bulletin of the Institute of Welding 61(5), pp. 123 – 133, **2017**. DOI: 10.17729/ebis.2017.5/14

[10] Moltasov, A. V. “A Study of the Stress State in Stress Concentration Zones under Tension of an Asymmetrically Reinforced Butt-Welded Joint”, Strength of Materials 49(5), pp. 718 – 725, **2017**. DOI: 10.1007/s11223-017-9917-x

[11] Tsumarev, Yu. A. “Effect of off-centre tensile loading on the stress state of butt-welded joints”, Welding International 25 (11), pp. 872 – 875, **2011**. DOI: 10.1080/09507116.2011.581426

[12] Lukianenko, A., Labur, T. M., Pokliatskyi, A. G., Motrunich, S., Bajic, D. “Investigation of fatigue strength and norms of emission of harmful substances in the air during MIG and TIG welding of 1460 aluminum-lithium alloy”, FME Transactions 47(3), pp. 608 – 612, **2019**. DOI: 10.5937/fmet1903608L

[13] Moltasov, A. V. “Application of the method of nonplanar sections to determine stresses in the zones of concentration caused by weld reinforcement in butt-welded joints”, Strength of Materials 45(1), pp. 116 – 122, **2013**. DOI: 10.1007%2Fs11223-013-9438-1

[14] Poklyatsky, A. G., Klochkov, I. N., Motrunich, S. I. “Some advantages of butt joints of thin wrought aluminum alloys AMg5M and AMg6M produced by FSW, compared to TIG-welded joints”, The Paton Welding Journal 7, pp. 16 – 21, **2015**. DOI: 10.15407/tpwj2015.07.03

[15] Moltasov, A. V. “Approximate calculation of radius of weld transition to base metal of welded butt joint according to normalized parameters”, The Paton Welding Journal 9, pp. 50 – 52, **2017**. DOI: 10.15407/tpwj2017.09.09

[16] Moltasov, A. V., Klochkov, I. N. “Calculation of the radius of transition of the weld to base metal of aluminum alloys welded joints”, The Paton Welding Journal 9, pp. 40 – 42, **2019**. DOI: 10.15407/tpwj2019.09.07

[17] Moltasov, A. V. “Stressed State of a Butt-Welded Joint with Regard for Displacements of the Centers of Inertia”, Materials Science 55 (3), pp. 358 – 366, **2019**. DOI: 10.1007/s11003-019-00310-2

[18] Herrera, H. H., Espinosa, R. G., Eras, J. J. C., Morejon, M. B. “Stress in butt welded joints of open profiles under torsion”, Engineering. Chilean Engineering Magazine, 23 (4), pp. 638 – 646, **2015**. DOI: 10.4067/S0718-33052015000400014 (in Spanish)